ARL-TR-9079 ● SEP 2020

DEVCOM ARMY RESEARCH LABORATORY

Self-Healing YSZ–Al2O3–(SiC, Nb2O5, Ta2O5) Thermal Barrier Coatings in a Corrosive Calcia–Magnesia–Alumina–Silicates Environment

by Bailey Ashmore, Michael J Walock, Anindya Ghoshal, and Muthuvel Murugan

NOTICES

Disclaimers

The findings in this report are not to be construed as an official Department of the Army position unless so designated by other authorized documents.

Citation of manufacturer's or trade names does not constitute an official endorsement or approval of the use thereof.

Destroy this report when it is no longer needed. Do not return it to the originator.

ARL-TR-9079 ● SEP 2020

Self-Healing YSZ–Al2O3–(SiC, Nb2O5, Ta2O5) Thermal Barrier Coatings in a Corrosive Calcia–Magnesia–Alumina–Silicates Environment

Bailey Ashmore
College Qualified Leaders, University of North Texas

Michael J Walock, Anindya Ghoshal, and Muthuvel Murugan
Vehicle Technology Directorate, CCDC Army Research Laboratory

REPORT DOCUMENTATION PAGE

Form Approved
OMB No. 0704-0188

1. REPORT DATE *(DD-MM-YYYY)*	2. REPORT TYPE	3. DATES COVERED (From - To)
September 2020	Technical Report	15 May–10 August 2019

4. TITLE AND SUBTITLE
Self-Healing YSZ–Al2O3–(SiC, Nb2O5, Ta2O5) Thermal Barrier Coatings in a Corrosive Calcia–Magnesia–Alumina–Silicates Environment

5a. CONTRACT NUMBER

5b. GRANT NUMBER

5c. PROGRAM ELEMENT NUMBER

6. AUTHOR(S)
Bailey Ashmore, Michael J Walock, Anindya Ghoshal, and Muthuvel Murugan

5d. PROJECT NUMBER

5e. TASK NUMBER

5f. WORK UNIT NUMBER

7. PERFORMING ORGANIZATION NAME(S) AND ADDRESS(ES)
CCDC Army Research Laboratory
ATTN: FCDD-RLV-P
Aberdeen, MD 21005

8. PERFORMING ORGANIZATION REPORT NUMBER
ARL-TR-9079

9. SPONSORING/MONITORING AGENCY NAME(S) AND ADDRESS(ES)

10. SPONSOR/MONITOR'S ACRONYM(S)

11. SPONSOR/MONITOR'S REPORT NUMBER(S)

12. DISTRIBUTION/AVAILABILITY STATEMENT
Approved for public release; distribution is unlimited.

13. SUPPLEMENTARY NOTES

14. ABSTRACT
Damage and open porosity are detrimental to the durability of the thermal barrier coatings (TBCs) used to protect the metallic components of gas turbine engines. These flaws lead to decreased thermal conductivity and increased oxygen diffusion, which result in uncontrollable growth of the thermally grown oxide, a common cause of TBC failure. To combat these defects, a self-healing additive can be distributed into the TBC matrix to provide as-needed closure of damage and pores. Another cause of TBC failure is the adherence and infiltration of calcia–magnesia–alumina–silicates (CMAS), which occurs in aircraft operating in particle-laden environments. This research is aimed to collect a fundamental understanding of the CMAS interaction with the proposed YSZ–Al_2O_3–(SiC, Nb_2O_5, Ta_2O_5) self-healing systems. These systems were exposed to high thermal-gradient experimentation and imaged using scanning electron microscopy and energy dispersion spectroscopy to examine CMAS's effects on the healing products and the systems' resistance to CMAS attacks.

15. SUBJECT TERMS
thermal barrier coating, TBC, sandphobic TBCs, gas turbine engines, blended TBC–ceramic composites, microstructure characterization, calcia–magnesia–alumina–silicates, CMAS, TBC–CMAS interaction

16. SECURITY CLASSIFICATION OF:			17. LIMITATION OF ABSTRACT	18. NUMBER OF PAGES	19a. NAME OF RESPONSIBLE PERSON
a. REPORT	b. ABSTRACT	c. THIS PAGE			Anindya Ghoshal
Unclassified	Unclassified	Unclassified	UU	21	19b. TELEPHONE NUMBER (Include area code) 410-278-7358

Contents

List of Figures

List of Tables

1. Introduction

Thermal barrier coatings (TBCs), typically made from 8-mole% yttria-stabilized zirconia (YSZ), are used in the hot sections of gas turbine engines to protect the nickel-based superalloy components from the extreme operating temperatures of 1300–1500 °C. YSZ has a low thermal conductivity and high thermal-expansion coefficient to help reduce heat transfer and stresses induced by the thermal-expansion mismatch among the metal substrate as well as good fracture toughness to help prevent the propagation of stress-induced cracks.[1]

The most common form of TBCs' failure is the spallation of the top coat from the bond coat due to the stresses induced by growth of the thermally grown oxide (TGO). This layer is the oxidation of the bond coat due to the diffusion of oxygen through the YSZ. The formation of the TGO is inevitable but is accelerated by the open porosity of the TBC and YSZ's transparency to oxygen.

To reduce the formation of the TGO, previous studies have shown the addition of Al_2O_3 decreases the thickness of the TGO as Al_2O_3 has a very slow oxygen-diffusion coefficient.[2,3] Al_2O_3 addition has also been shown to increase the bond strength to the NiCrAlY bond coat.[2] Implementing a self-healing ability into TBCs shows potential to further restrict the TGO's growth by providing as-needed closure to unwanted porosity. This ability is achieved by distributing the self-healing system into the matrix where it remains insulated and unreacted until exposed to oxygen and elevated temperatures, which trigger the healing reaction.

The healing process results from the formation of a product with greater volume to fill in the crack. Theoretically, the volume expansion can be calculated using Eq. 1.[4]

$$V_{self-healing} = \frac{(M_{product})(\rho_{additive})}{(M_{additive})(\rho_{product})} - 1\ . \tag{1}$$

Where $V_{self\text{-}healing}$ is the percent of expansion, $M_{product/additive}$ is the molar mass of the product or additive and $\rho_{product/additive}$ is the density of the product or additive. These values can be found in the Appendix. The self-healing additives in this work are silicon carbide (SiC), niobium pentoxide (Nb_2O_5), and tantalum pentoxide (Ta_2O_5).

When exposed to oxygen at high temperatures, SiC forms SiO_2, expanding 118%, assuming complete oxidation.[4] The Ta_2O_5 healing additive reacts with Al_2O_3 to form aluminum tantalate ($AlTaO_4$) when exposed to elevated temperatures. When using the same expansion ratio, the reaction ratios of Ta_2O_5 to $AlTaO_4$ and Al_2O_3 to $AlTaO_4$ are considered. The calculated volume expansion of this reaction is 43%. For the Nb_2O_5, like Ta_2O_5, both reactions are considered calculating a 59% volume expansion.

It is important the additive as well as the healing product be thermomechanically compatible with the TBC matrix and harsh engine environment.

Military rotorcraft operating in particle-laden environments such as deserts, urban canyons, and volcanic areas do so at a heightened risk of power loss and engine failure resulting from calcia–magnesia–alumina–silicates (CMAS) attacks on the TBC. Sand, dust, and ash enter the gas turbine engines and melt under the high temperature of the combustion section. This molten sand then adheres to the TBC and infiltrates into the porous structure, decreasing the designed strain tolerance as well as chemically reacting with the YSZ, leaching out the yttria to destabilize the tetragonal to monoclinic.[5]

For any proposed TBC it is vital to understand how the coating will perform in such environments. We know the selected systems will form the healing product to restore physical damage, but little is known of their resistance to the chemical damage inflicted by the CMAS. This research is aimed to collect a fundamental understanding of the interactions these coating have in a high-temperature CMAS environment.

2. Methods

The TBC matrix for these systems consisted of YSZ and Al_2O_3 powders (SkySpring Nanomaterials, Inc.) with additives SiC (SkySpring), Ta_2O_5 (Alfa Aesar), and Nb_2O_5 (Alfa Aesar). Sample compositions are as listed in Table 1. Each system was pressed into 1.25-inch-square molds then sintered at 1500 °C for 4 h to preform the self-healing product to examine CMAS interaction.

Table 1 Sample composition

Coating	Weight percent YSZ	Weight percent Al_2O_3	Weight percent additive
YSZ	100	0	0
YSZ–Al_2O_3–6-wt% SiC	56	38	6
YSZ–Al_2O_3–20-wt% SiC	70	10	20
YSZ–Al_2O_3–Ta_2O_5	56	12	32
YSZ–Al_2O_3–Nb_2O_5	56	12	32

Omega OV-1-20-k-12 thermal couples were mounted to the samples using Cotronics Corp Resbond 907GF putty to collect comparative data of the effects the additive has on thermal conductivity. A slurry was made with AFRL-02 and applied to half of the surface of each sample for the CMAS-exposed systems and allowed to dry for 24 h. Prepared samples were exposed to short-term cyclic testing under a

high thermal gradient, using the Sand-modified ablation rig tester with a target temperature of 1500 °C for two cycles (5 min *in*/5 min *out*).

Portions of the thermally exposed samples were mounted in epoxy and polished for cross-sections.

The microstructure and chemical analysis of the surface and cross-section of systems with and without CMAS exposure were examined using scanning electron microscopy (SEM) (Hitachi SU3500) and energy dispersion spectroscopy (EDS) (Bruker).

3. Results and Discussion

3.1 YSZ–Al_2O_3–6-wt% SiC

Under a 6-wt% SiC system, extensive surface damage was observed. Thermal exposures resulted in further sintering while the addition of sand led to the formation of Si-rich regions. Figure 1 shows the ZrO_2–SiO_2 phase diagram and the formation of $ZrSiO_4$ can occur with only small additions of SiO_2.[6] When analyzing the EDS images of the pretested and thermal-exposed without sand sample, seen in Fig. 2a, b, d, and g, we see clear grains mapping overlap of Si and Zr, suggest the formation of zirconia ($ZrSiO_4$).With the addition of sand we no longer detect these $ZrSiO_4$ regions and now observe the silicon only in areas of high CMAS concentration, suggecting the silicon was dissolved out and reprecipitated into the large CMAS formations seen in the bottom portion of Fig. 2f and g.

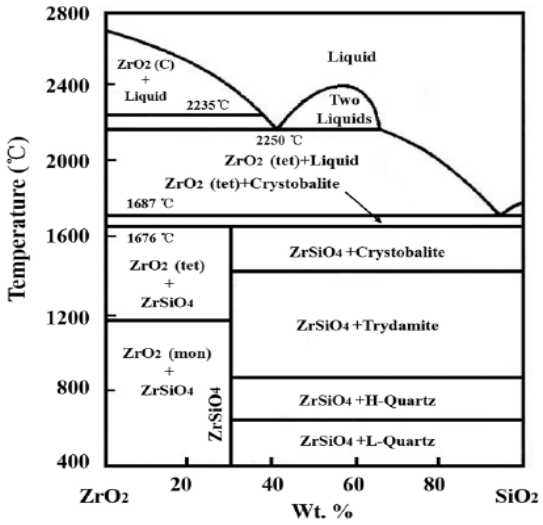

Fig. 1 ZrO_2–SiO_2 phase diagram (from *Materials* journal[6])

With thermal exposure this system also presented extensive surface damage forming large cracks along the surface, as seen in Fig. 2b.

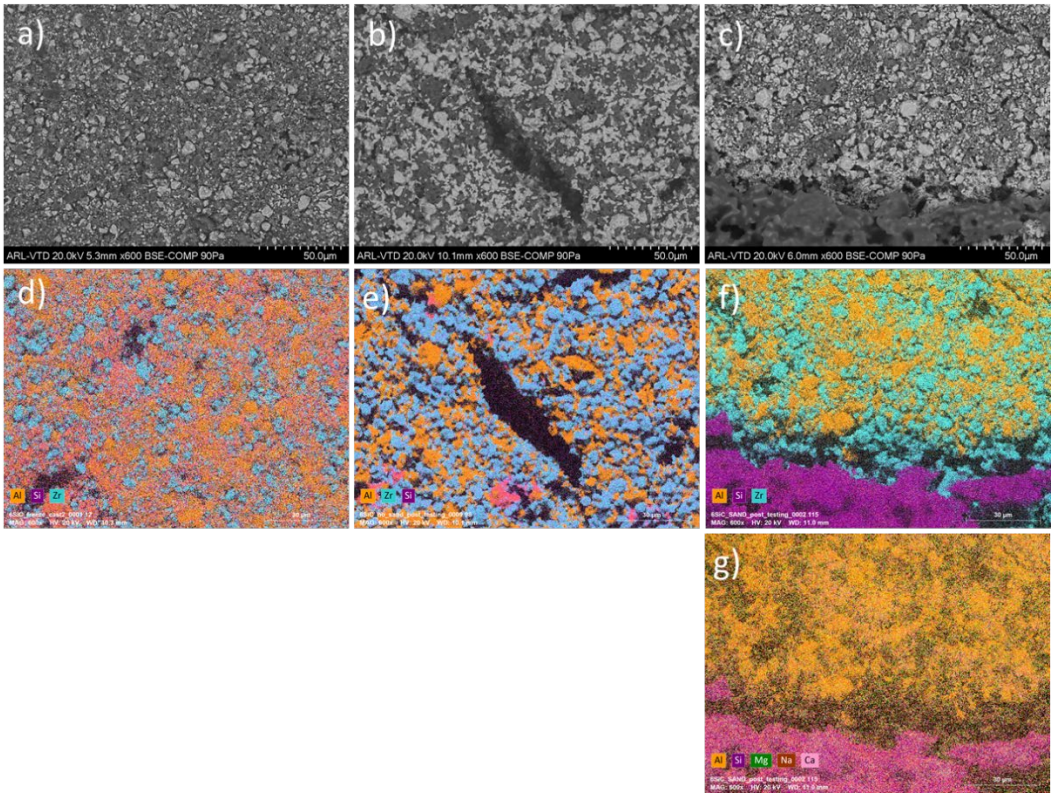

Fig. 2 YSZ–Al_2O_3–6-wt% SiC a) pretested SEM, b) thermally exposed without sand, and c) thermal exposure with sand; SEM images d) pretested, e) without sand, and f) with sand EDS present Al, Si and Zr; and g) sand exposure EDS presenting CMAS elements

3.2 YSZ–Al_2O_3–20-wt% SiC

SEM imaging suggests the 20-wt% SiC system is more porous than the 6-wt% SiC system with the structure presenting more surface voids. This system also shows increased sintering attributed to the addition of SiC lowering the melting temperature closer to the eutectic temperature.

The addition of sand leads to widespread segregation and reprecipitation of the different components of the system as seen in Fig. 3c and f.

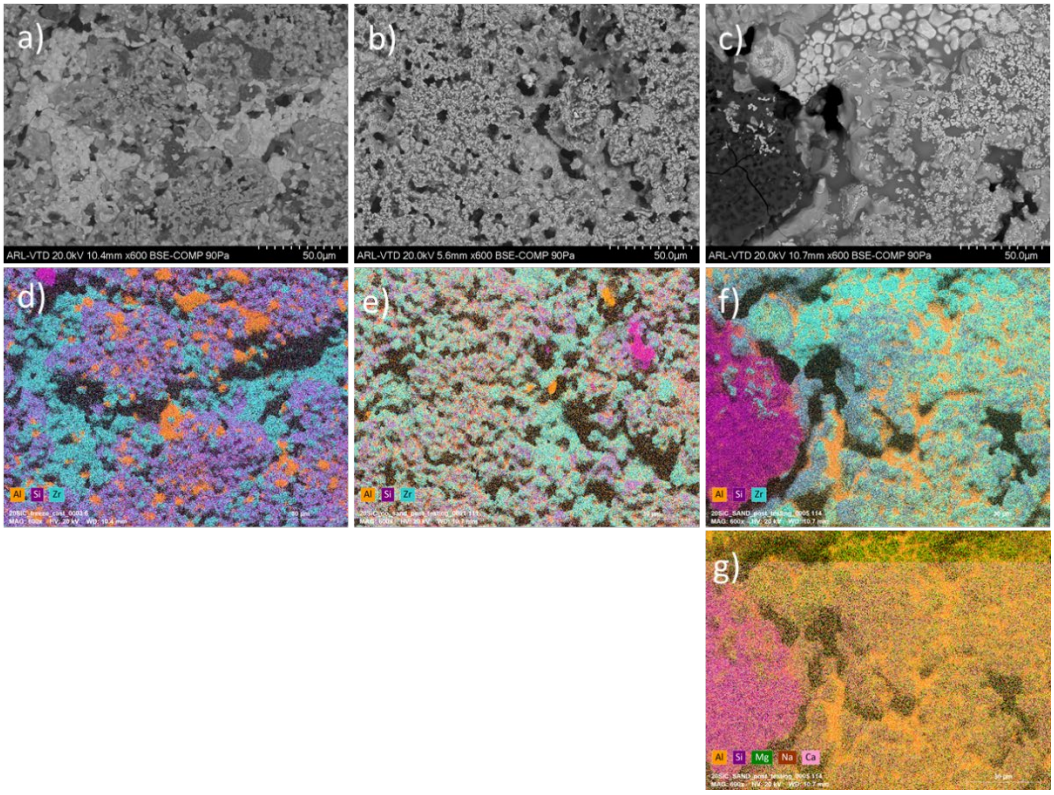

Fig. 3 YSZ–Al_2O_3–20-wt% SiC a) pretested, b) thermally exposed without sand, and c) thermal exposure with sand; SEM images d) pretested, e) without sand, and f) with sand EDS present Al, Si and Zr; and g) sand exposure EDS presenting CMAS elements

Cross-sectional SEM and EDS images of the sand-exposed system show widespread elemental segregation continues. In the EDS images we see the formation of $ZrSiO_4$ in the purple regions in Fig. 4 and needle-like formations in pink in areas between the $ZrSiO_4$. These needle-like formations were assumed to be mullite ($3Al_2O_2$ $2SiO_2$), but EDS shows these areas have high concentrations of yttrium, so further testing such as with X-ray diffraction is required to determine this compound.

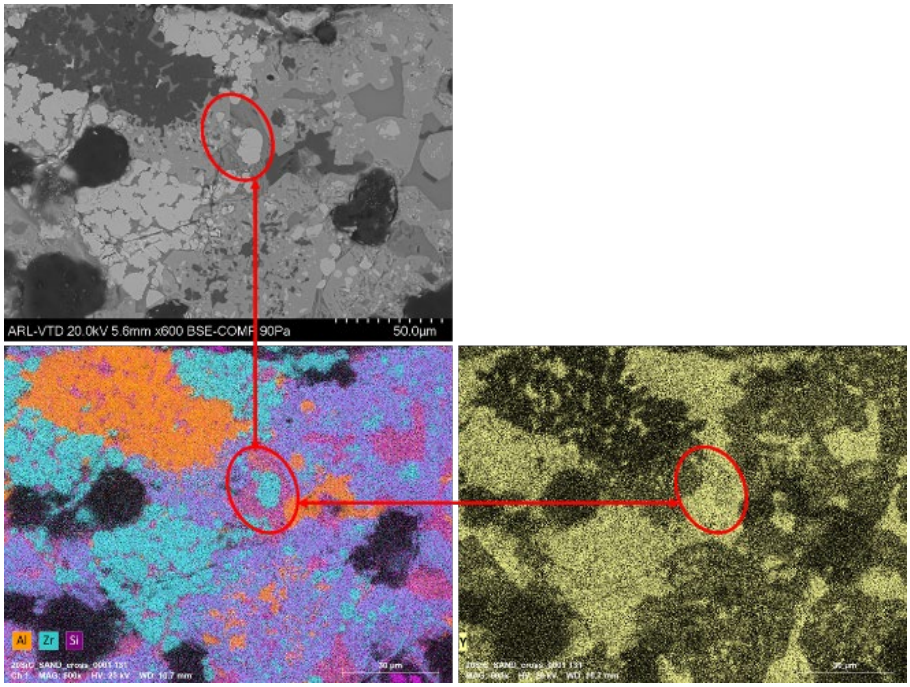

Fig. 4 Images shows mullite formations contain higher concentrations of Y

Figure 5 also shows the exposure to sand results in the delamination of the surface under a glassy CMAS formation, suggesting poor resistance to CMAS attack.

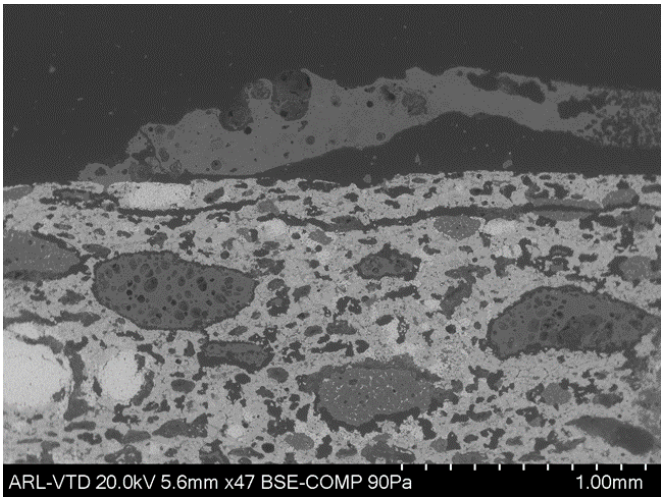

Fig. 5 SEM image of CMAS-exposed 20-wt% system's delamination of the surface

3.3 YSZ–Al_2O_3–Ta_2O_5

Under the Ta_2O_5 system, the self-healing product $AlTaO_4$ is assumed to the regions with higher concentrations of Al and Ta, seen in Figs. 6 and 7. These regions have separated from the surrounding material and Zr–Nb-rich flake structures can be seen in areas surrounding $AlTaO_4$ shown in magnification in Fig. 6e and g. These

structures continue throughout the sample as seen in a cross-sectional image (Fig. 7).

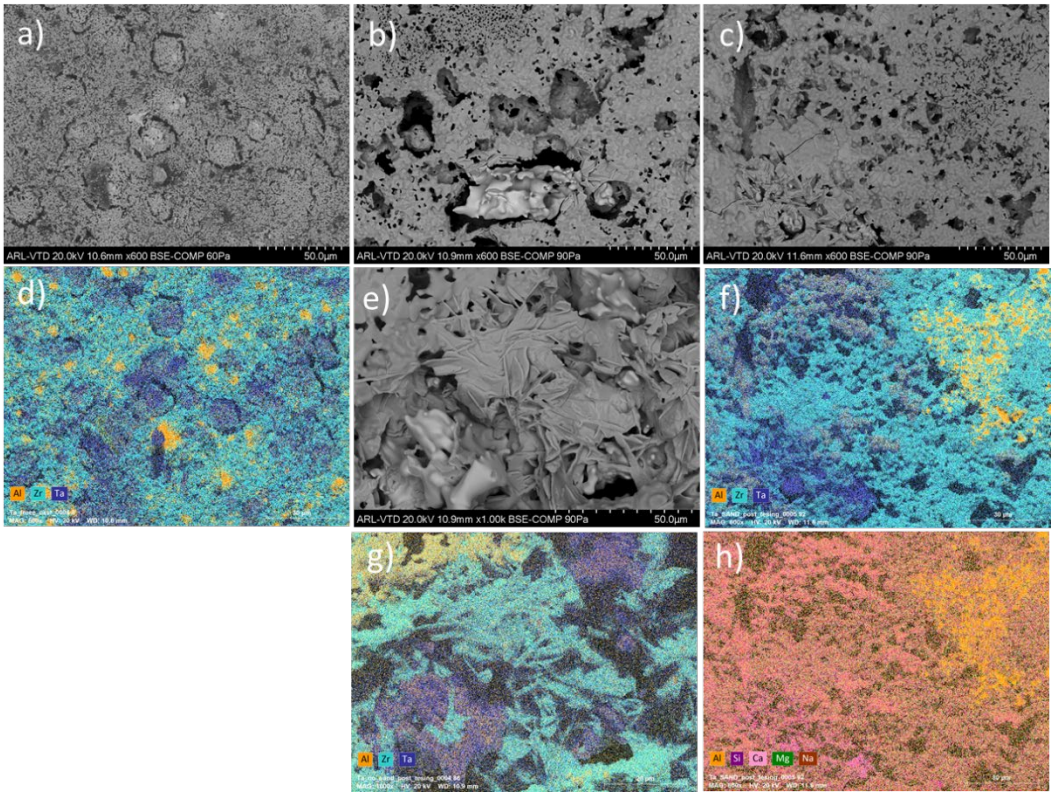

Fig. 6 YSZ–Al_2O_3–Ta_2O_5 pretested in a) SEM and d) EDS images; thermal exposures without sand b) at 600×, e) at 1000× magnification of Zr–Ta flakes SEM, and g) EDS of Zr–Ta flakes; and thermally exposed with sand in c) SEM, f) EDS of system elements, and h) EDS showing CMAS elements

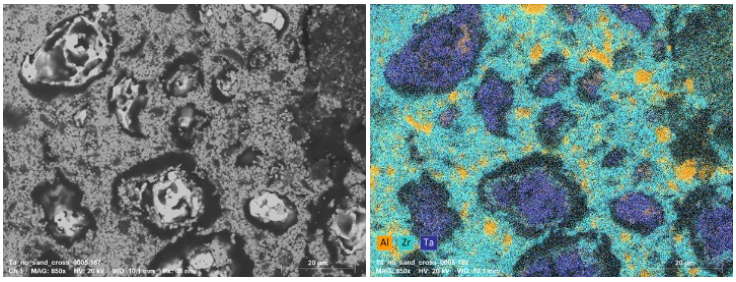

Fig. 7 Cross-sectional SEM (left) and EDS images showing Zr–Nb flakes surrounding $AlTaO_4$

The second phenomena seen in this system are the changes in Al_2O_3 distribution along the surface with the addition of sand. In the EDS images in Fig. 8c and d, Al is detected in the area of orange. Without sand, Al is detected in spherical grains,

evenly distributed throughout the presented region. With sand, Al is detected in rod-shaped indentions along the surface.

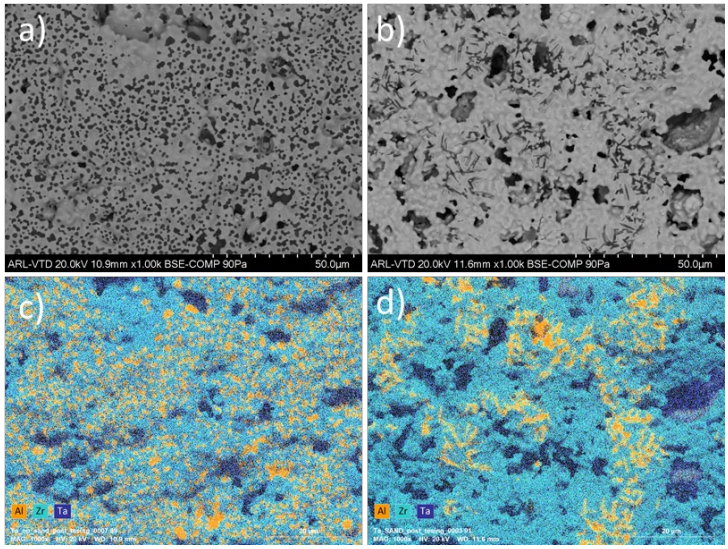

Fig. 8 SEM a) and EDS c) images show Al distributions of exposures without sand, while SEM b) and EDS d) images show distribution of exposures with sand

To determine the possible origin of these indentions cross-sections were observed just below the surface (Fig. 9). Branch and needle-like structures with a high concentration of Al are seen in areas with high concentrations of CMAS. Rigid, rectangular shapes were seen with concentrations of yttria, suggesting yttria has been leached out of the YSZ through its interaction with CMAS.

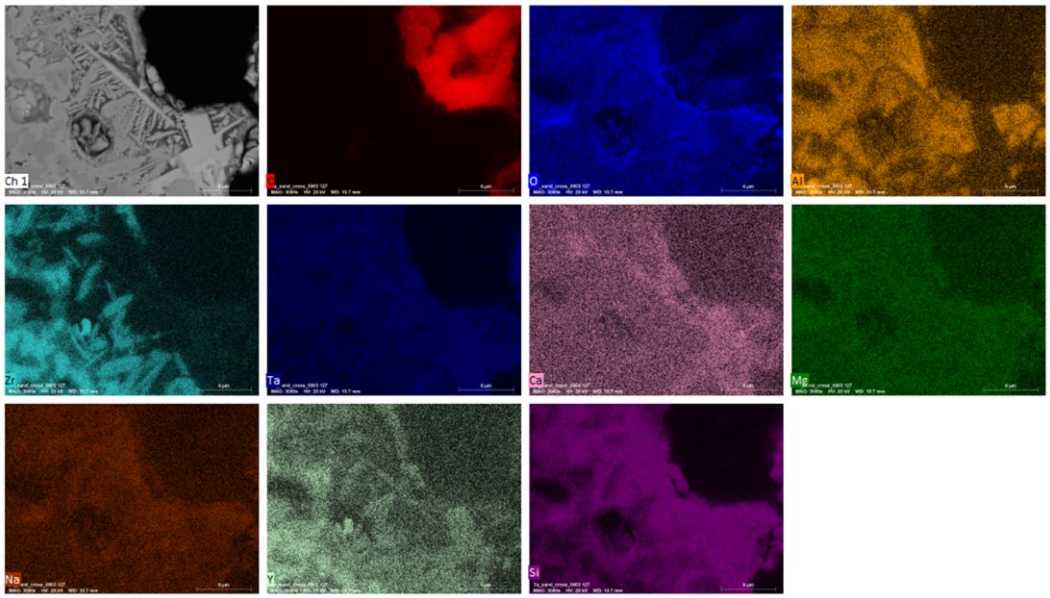

Fig. 9 EDS mapping of rigid features found in the cross-section below surface

3.4 YSZ–Al_2O_3–Nb_2O_5

Pretested images (Fig. 10) show small, evenly distributed grains of Zr and Nb and porous clusters of Al_2O_3.

Figure 10b displays the formations of aluminum niobate, rod-like grains that share similar shape and size to those seen in previous studies,[7,8] as well as the formation of irregular scoop-like zirconium niobate grain. In regions containing zirconium niobate, Al_2O_3 forms clearly separated clusters suggesting Al_2O_3 is insoluble in zirconium niobate.

For the sand-exposed system, saw-tooth-like $AlNbO_4$ structures formed at the grain boundaries of the irregular zirconium niobate grains.

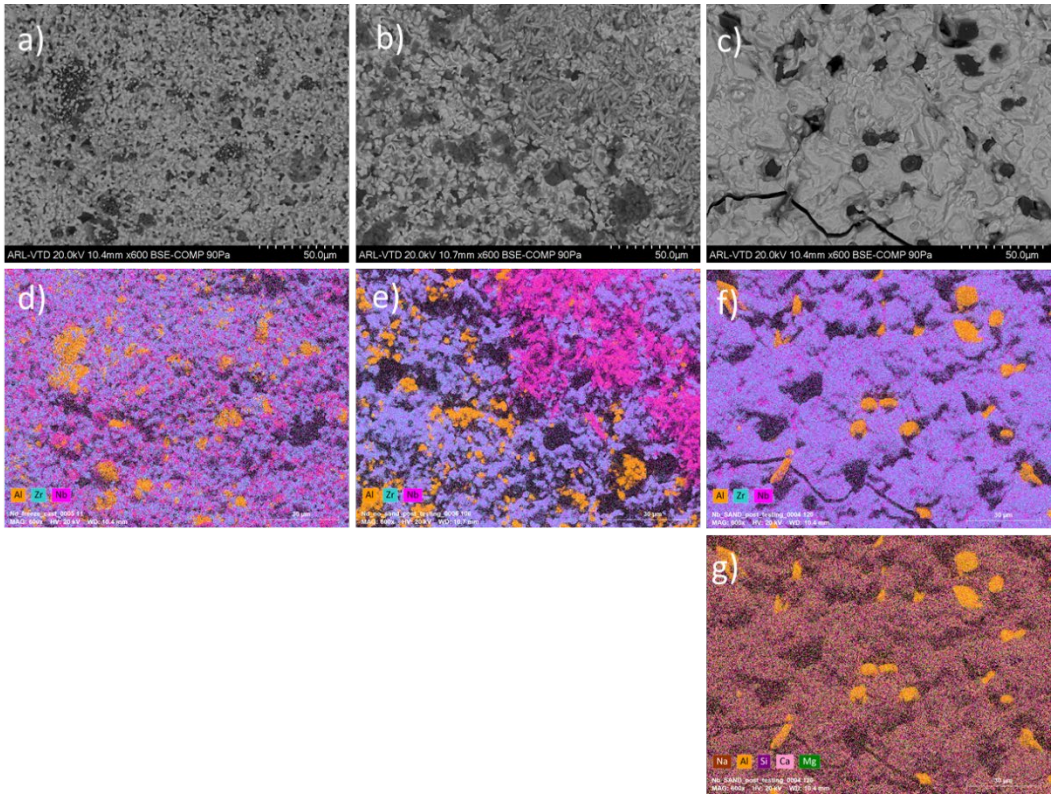

Fig. 10 YSZ–Al_2O_3–Nb_2O_5 system a) pretested, b) thermally exposed without sand, and c) thermal exposure with sand in SEM images; d) pretested, e) without sand, and f) with sand in EDS images presenting Al, Si, and Zr; and g) sand exposure in EDS presenting CMAS elements

4. Conclusion

When comparing the SEM and EDS images of the four systems it can be concluded that testing performed at 1500 °C induces structural damages and new phase formation. The following suggests poor CMAS resistance at such extreme temperatures:

- The SiC systems presented large phase separation and surface cracks and delamination.
- The Ta_2O_5 system showed an increased porosity after thermal exposures due to the contraction of the $AlTaO_2$ healing-product formations separating from their surroundings. The surrounding voids have spars formation of an unexpected zirconia tantalate, and CMAS regions show formations with increased detections of yttrium suggesting a successful chemical attack of the CMAS.
- Under the Nb_2O_5 system, thermal exposures led to the formation of a zirconium niobate. No extensive damage was observed so this system seems to show the most promise; further testing is required to identify these formations to determine if they possess the required properties for a TBC.

5. References

1. Padture NP, Gell M, Jordon EH. Thermal barrier coatings for gas-turbine engine applications. Science. 2002;296:280–284.
2. Keyvani A, Saremi M, Heydarzadeh-Sohi M. Oxidation resistance of YSZ-alumina composites compared to normal YSZ TBC coatings at 1100 °C. J All Comp. 2011;509:8370–8377.
3. Afrasiabi A, Saremi M, Kobayashi A. A comparative study on hot corrosion resistance of three types of thermal barrier coatings: YSZ, YSZ + Al2O3 and YSZ/Al2O3. Mat Sci Eng. 2008;478:264–269.
4. Ouyang T, Xiong S, Zhang Y, Liu D, Fang X, Wang Y, Feng S, Zhou T, Suo J. Cyclic oxidation behavior of SiC-containing self-healing TBC systems fabricated by APS. J All Comp. 2017;691:811–821.
5. Vidal-Setif MH, Chellah N, Rio C, Sanchez C, Lavigne O. Calcium–magnesium–alumino–silicate (CMAS) degradation of EB-PVD thermal barrier coatings: characterization of CMAS damage on ex-service high pressure blade TBCs. Surf Coat Tech. 2012;208:39–45.
6. Liu L, Ma Z, Yan Z, Zhu S, Gao L. The ZrO2 formation in ZrB2/SiC composite irradiated by laser. Materials. 2015;8:8745–8750.
7. Chen L, Hu M, Feng J. Mechanical properties, thermal expansion performance and intrinsic lattice thermal conductivity of AlMO4 (M=Ta, Nb) ceramics for high-temperature applications. Ceram Int. 2019;45:6616–6623.
8. Zhang X, Zhou J, Wu C, Chuanying L. Preparation and characterization of Nb2O5-Al2O3 system ceramics with different Al2O3 additions. Key Eng Mat. 2013;544:60–63

Appendix. Materials' Percent of Expansion Values

In Table A-1 **t**he volume expansion is calculated using Eq 1 in the main report. $V_{self\text{-}healing}$ is the percent of expansion, $M_{product/additive}$ is the molar mass of the product or additive**,** and $\rho_{product/additive}$ is the density of the product or additive.

Table A-1 Percent of expansion values

Material	Molecular weight (g/mol)	Density (g/cm^3)
SiC	40.10	3.20
SiO_2	60.08	2.20
Al_2O_3	101.96	3.95
Ta_2O_5	441.89	8.20
$AlTaO_4$	271.93	6.42
Nb_2O_5	265.81	4.60
$AlNbO_4$	200.83	4.35

List of Symbols, Abbreviations, and Acronyms

Al	aluminum
CMAS	calcia–magnesia–alumina–silicates
EDS	energy dispersion spectroscopy
SEM	scanning electron microscopy
TBC	thermal barrier coating
TGO	thermally grown oxide
YSZ	yttria-stabilized zirconia

1 (PDF)	DEFENSE TECHNICAL INFORMATION CTR DTIC OCA
1 (PDF)	CCDC ARL FCDD RLD CL TECH LIB
7 (PDF)	CCDC ARL FCDD RLV P A GHOSHAL M. MURUGAN M WALOCK L BRAVO R EMERSON C MOCK M PEPI
2 (PDF)	CCDC AVMC R ARMSTRONG K KERNER
4 (PDF)	NAVAIR L SCHMIDT C ROWE C MYERS J SCITTORE
4 (PDF)	AIR FORCE RSRCH LAB R SIKORSKI A KATZ D LEE R SONDERGAARD